



OPEN ACCESS

EDITED BY

Paolo Gargiulo,
Reykjavik University, Iceland

REVIEWED BY

Jonathan Charles Jarvis,
Liverpool John Moores University,
United Kingdom
Sandeep Kumar Mishra,
Yale University, United States

*CORRESPONDENCE

Karla P. García-Pelagio
✉ kpaolag@ciencias.unam.mx

RECEIVED 23 April 2024

ACCEPTED 19 July 2024

PUBLISHED 07 August 2024

CITATION

Martínez-Gutiérrez B and García-Pelagio KP (2024) Infrared thermography and computed tomography imaging for hind limb study after immobilization-induced disuse atrophy. *Front. Imaging*. 3:1421979. doi: 10.3389/fimag.2024.1421979

COPYRIGHT

© 2024 Martínez-Gutiérrez and García-Pelagio. This is an open-access article distributed under the terms of the [Creative Commons Attribution License \(CC BY\)](#). The use, distribution or reproduction in other forums is permitted, provided the original author(s) and the copyright owner(s) are credited and that the original publication in this journal is cited, in accordance with accepted academic practice. No use, distribution or reproduction is permitted which does not comply with these terms.

Infrared thermography and computed tomography imaging for hind limb study after immobilization-induced disuse atrophy

Berenice Martínez-Gutiérrez^{1,2} and Karla P. García-Pelagio^{1,2*}

¹Department of Physics, Universidad Nacional Autónoma de México School of Science, Mexico City, Mexico, ²Laboratory of Muscle Mechanobiology, Universidad Nacional Autónoma de México School of Science, Mexico City, Mexico

Immobilization for treatment after an injury can lead to disuse atrophy, resulting in reduced functionality and strength of the immobilized limb. In our study, we utilized infrared thermography (IR) and computed tomography (CT) *ex vivo* to assess both physiological and structural changes following hind limb immobilization in a young Wistar rat model. Twelve rats weighing 275 ± 30 g had their right hind limbs immobilized with a modified Thomas-splint for varying durations (3, 7, or 14 days). IR imaging using an infrared camera provided insight into limb temperature changes. For micro-CT, we implemented a stain-ethanol fixation method and a gray score which enabled us to visualize and quantify muscle alterations. Thermographic images showed an increase in temperature of up to 8% in the hind limb at supine position at 14 days due to the inflammatory process while micro-CT exhibited muscle shrinkage of 10 and 18% at 7 and 14 days, respectively. Our findings underscore the efficacy of IR and micro-CT as rapid and precise imaging modalities for detecting morphological shifts in muscle tissue, particularly in pathological conditions like atrophy.

KEYWORDS

X-rays, muscle atrophy, infrared image, animal models, skeletal muscle physiology

Introduction

Immobilization is one of the most common treatments for lower extremity injuries, such as fractures, arthrodesis or arthralgia, playing a pivotal role in aiding patient recovery. However, its prolonged application can precipitate musculoskeletal complications such as disuse muscle atrophy. This condition, characterized by a decline in skeletal muscle strength and function, necessitates extensive rehabilitation (Booth, 1987; Dupont et al., 2003; Clark et al., 2010; Crossland et al., 2019). Therefore, it becomes necessary to explore the effects of immobilisation on skeletal muscle using non-traditional medical imaging techniques.

Thermography, a rapid, non-invasive imaging technique, captures the infrared radiation emitted by a body and correlates it with a physiological response (dos Santos Bunn et al., 2020; Kesztyüs et al., 2023). This response is intricately linked to the complex dynamics governing heat exchange processes among the skin, internal tissues, local vasculature, metabolic activity, and sympathetic and parasympathetic activity regulation to maintain homeostasis (Al-Nakhli et al., 2012).

Its versatile applications span from diagnosing inflammatory lesions (Aboushady et al., 2021; Cantillo-Negrete et al., 2021) and diabetes (Nishide et al., 2009; Thirunavukkarasu et al., 2020) to analyzing circulatory and microcirculatory alterations (Ilo et al., 2020) and even aiding in the assessment of rheumatoid arthritis (Tan et al., 2020).

In our study, temperature differences may indicate tissue inflammation (Zaproudina et al., 2006; Al-Nakhli et al., 2012; dos Santos Bunn et al., 2020), potentially signaling the onset of muscle atrophy (Huang et al., 2019).

Computed Tomography (CT) is one of the most widely used non-invasive and non-destructive imaging modalities (Boerckel et al., 2014) employed post-injury or in tumor assessments because it is a fast and inexpensive technique compared to other studies such as magnetic resonance or nuclear medicine (Edmund and Nyholm, 2017; Florkow et al., 2022; Hussain et al., 2023). It provides detailed images of the bones, muscles, fat, organs, and blood vessels facilitating the detection of angiogenesis and organ or tissue damage (Strandberg et al., 2010; Engelke et al., 2018; Polyaev et al., 2018; Tolonen et al., 2021; Findakly et al., 2023).

While highly mineralized structures like bones provide excellent contrast owing to their significant attenuation of X-rays, soft tissues present a challenge. Their poor X-ray attenuation leads to minimal X-ray absorption, with attenuation coefficients similar to water. Consequently, this results in low contrast between internal features, presenting a significant challenge in imaging soft tissues accurately (Lusic and Grinstaff, 2013).

Low-density tissues, like fat and muscle, exhibit a lower concentration of atoms per unit volume compared to high-density tissues. Rich in lighter elements such as carbon, hydrogen, and oxygen, these tissues attenuate X-rays poorly, resulting in diminished contrast between internal features. On the other hand, high-density tissues, such as bone or certain metal implants, have a higher atom concentration per unit volume. These tissues often comprise heavier elements like calcium, phosphorus, and metals, leading to more effective X-ray attenuation (O'Sullivan et al., 2018). The expression that relates the X-rays absorption and atomic number is: $\mu \approx \rho Z^4 / AE^3$ where μ is the X-ray absorption coefficient, ρ is the material's density, Z is the atomic number, A is the atomic mass and E is the X-ray energy (Kalender, 2005).

In X-ray imaging, these disparities in tissue density and composition are used to generate contrast between various structures within the body. X-rays interact differently with tissues of varying densities, enabling the visualization of bones, organs, and other anatomical structures in CT scans.

To meet the challenge that low-density tissues present, radiopaque contrast agents are frequently utilized to amplify signal intensity in X-ray imaging. CT sensitivity is enhanced, facilitating clearer differentiation between tissues. This enhancement provides crucial biochemical insights into the tissue, enabling a more thorough evaluation (Lusic and Grinstaff, 2013; Descamps et al., 2020). Contrast media play a pivotal role in various medical imaging procedures, offering enhanced visualization of anatomical structures and physiological processes with certain drawbacks. They can be costly, challenging to administer, and may not always exhibit a well-defined biodistribution and pharmacokinetic profile. Furthermore, some of these agents may suffer from solubility issues

or form unstable suspensions leading to high viscosity. Moreover, their ability to consistently penetrate tissues may vary (Lusic and Grinstaff, 2013; Cormode et al., 2014).

Contrast media can be categorized according to their molecular weight (MW). Those with low MW, such as iodine ionic or non-ionic based agents (Sachse et al., 1997; Hallouard et al., 2010; Ayala-Domínguez and Brandan, 2018). And, on the other hand, high MW contrast agents, also known as blood pool agents for their prolonged circulation times within the bloodstream, include nanoparticles, nanosuspensions, nanocapsules or liposomal iodinated contrast agents (Barret et al., 2006; Lalwani et al., 2013; Lusic and Grinstaff, 2013; Cormode et al., 2014). The most commonly used contrast agents for visualizing soft tissue, both *in vivo* or *ex vivo*, are iodine-based agents [such as potassium iodide (I_2KI), iohexol, ioxaglate, iopromide, iothalamate, iodixanol, iomeron or iopamidol]. These agents are preferred for their ability to provide high-resolution imaging and deep tissue penetration through the interaction with biological structures. However, they come with disadvantages including non-specific biodistribution, high osmolality, high viscosity, and the potential for toxicity when administered in high concentrations leading to adverse physiological effects and even tissue shrinkage (Pasternak and Williamson, 2012; Lusic and Grinstaff, 2013; Vickerton et al., 2013; Boutin et al., 2016; Lortie et al., 2022). Other researchers have explored alternative contrast agents like polymerising agents, glutaraldehyde, osmium tetroxide, iodine in ethanol, phosphotungstic acid, or formalin for *ex-vivo* visualization of skeletal muscle. However, these alternatives also present some limitations including complexity in use, limited tissue penetration or toxicity (Johnson et al., 2006; Metscher, 2009; Rolls, 2011; Vickerton et al., 2013; Schaad et al., 2017; Leonard et al., 2021). Consequently, alternative staining methods for micro-CT such as ethanol, was investigated as viable, easy-to-use, and affordable options for *ex-vivo* applications (Lusic and Grinstaff, 2013; Dudak et al., 2016; Patzelt et al., 2019; Descamps et al., 2020; Leonard et al., 2021).

Therefore, this study aims to validate rapid, cost-effective techniques, thermography and micro-CT imaging, by quantifying the physiological and structural changes in rat hind limbs following immobilization-induced disuse atrophy.

Methods

Animals

We used twelve young Wistar male rats (275 ± 30 g) provided by the UNAM-School of Sciences Animal Facility for all studies reported here. Before each protocol, animals were anesthetised with 4–5% isoflurane in an induction chamber and maintained with 2% isoflurane combined with oxygen at 0.8 l/min (14.7 psi) using a precision vaporiser (Vet Equip Inc. USA). Rats were divided into three-groups depending on the unilateral hind limb immobilization time (Imm): three (3 d), seven (7 d), or 14 days (14 d) ($n = 4$ for each group). The contralateral non-Imm limb served as the control (C) group. Throughout the immobilization process, a heat lamp was used to maintain the animals' warmth. All experimental protocols

were conducted in accordance with the regulations stipulated by the Institutional Animal Care and Use Committee (IACUC) of the School of Sciences-UNAM, adhering to the guidelines outlined in the Mexican Official Norm (NOM-062-ZOO-1999).

Modified Thomas-splint immobilization

We utilized a modified Thomas splint technique, supplemented with a plaster cast for effective immobilization. Under anesthesia, we employed a rapid-drying adhesive spray (Q.D.A. Spray, Cramer, USA) on the right hind limb, followed by the application of under-wrapped strips (7 × 20 cm, Cramer) from the phalanges to the femur, just below the pubis, to preserve fur and safeguard the skin. Athletic sport tape 1050i (Cramer) was promptly used to secure the bandage in place. A custom-made modified Thomas splint (Robinson and O'Meara, 2009) was tailored for each limb, ensuring a snug fit to prevent edema or removal by the animal. This splint consists of a 22-gauge copper wire ring encircling the mid-femur and hip area, with two metal shafts forming a long U-shape extending down the sides of the limb to the middle of the phalanges (Figure 1A). After securing the splint, additional tape was applied to reinforce its position, followed by the application of a plaster bandage from distal to proximal on the hind limb, maintaining the toe in a plantar-flexion position at an angle between 30 and 40 degrees while keeping the knee straight. This position induced mild atrophy in the limb. A drying period of 10–15 min was allowed before returning the animal to its cage, where they could move freely using their left hind limb and both forelimbs. Daily monitoring for signs of plaster damage, swelling, irritation, or gait issues was conducted, and any deterioration or plaster chewing prompted cast replacement while ensuring continuous immobilization with the splint. Animals had *ad libitum* access to food and water, with no notable differences in food intake observed during immobilization.

Infrared thermography

Prior to each image acquisition, the infrared (IR) camera (Fluke TiS60+, USA) underwent calibration using a multimeter thermocouple (Keithley 2110-120, USA) and self-camera calibration option, ensuring accuracy within a range of 22–35°C, with an emissivity point of 0.98 ± 0.05 , thermal sensitivity of <30 mK and operated at a frequency acquisition rate of 60 Hz, as detailed in previous studies (Lahiri et al., 2012; Faraji et al., 2022). Maintaining strict environmental control, the experimental room was set at $23 \pm 0.5^\circ\text{C}$, and uniform LED lighting to minimize infrared interference. The IR camera was placed at a distance of 50 cm perpendicular to the animal, ensuring optimal imaging conditions.

Under anesthesia, the cast was gently removed from the right limb, ensuring minimal disturbance, afterwards the animal was carefully positioned on an insulated surface with their extremities securely taped down. A 15-min acclimation period ensued to stabilize the animal's temperature and mitigate any thermal background disruptions post-cast removal or animal

manipulation. Subsequently, thermograms of non-immobilized (C) and immobilized at 3, 7, and 14 d were captured, in both prone and supine positions and analyzed with SmartView software (Fluke, v 4.4) utilizing a high-contrast palette within the 22–35°C range.

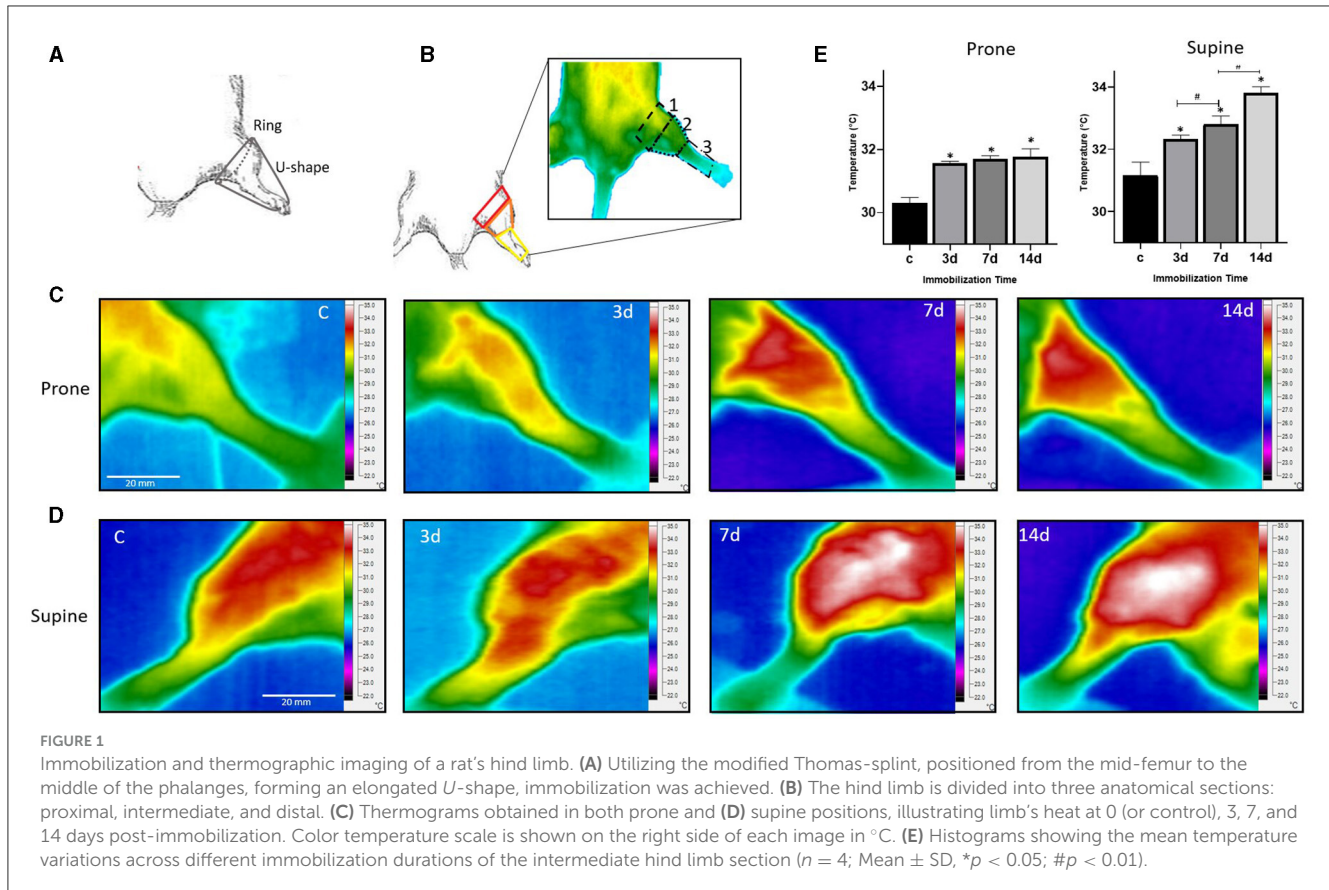
In the supine position, attention was set to the tibialis anterior (TA), whereas in the prone position, in the gastrocnemius muscle. Three regions of interest (ROI) were defined according to anatomical landmarks, partitioning the limb into three sections (Figure 1B): (1) the proximal region, from the limb's onset to an imaginary straight line extending from the base of the tail; (2) an intermediate section demarcated by the proximal region and the knee; and (3) the distal segment, encompassing the area between the termination of Section 2 and the ankle.

Separately, the limbs of three non-Imm rats were analyzed and compared with the experimental non-Imm limb, revealing no statistically significant disparities, thus validating the contralateral limbs as a control (C).

Micro-CT images

Hind limb staining

After the IR images were taken, the animals were euthanised. Both hind limbs were removed from the animal and the fur was completely pulled out from proximal (insertion of the head of the femur) to distal (to the toe). Fur removal was carefully performed assuring that the limb musculature remains intact. Two stain-fixation protocols were used to determine which provided the best image between C and Imm hind limb under *ex vivo* conditions: (1) 100 % ethanol at different time points (3, 5, 7, and 14 days) or (2) an ascending ethanol concentration of 25, 50, 75% for 12 h each (Shirai et al., 2014). Following these protocols, CT images were acquired using a micro-CT (SkyScan 1276, Bruker, Germany) calibrated to water at 40 kV, 150 μA , no filter, step and shoot mode, rotation step 0.4° , pixel size of 14 μm and $4,018 \times 2,016$ matrix, reconstructed and analyzed using CTan software (Bruker, v 1.19). Raw images were displayed in a palette of 255 channels representing gray intensity levels. On each acquired image, a volume of interest of 20 slices was delineated by placing a 250-pixel circular region of interest (ROI), and then the linear attenuation coefficient was calculated three times in each region (Yan et al., 2012; Hakki et al., 2021). To know which stain-fixation protocol gave the best image quality, the contrast-to-noise ratio (CNR) was calculated using the following equation: $\text{CNR} = \text{ROI}_1 - \text{ROI}_2 / [1/2 (\text{SD}_1^2 + \text{SD}_2^2)]^{1/2}$ (Bushberg and Boone, 2011; Pauwels et al., 2014). Where ROI_1 is the value of the muscle tissue area and ROI_2 is the muscle surrounding area, SD_1 and SD_2 correspond to the respective standard deviations. CNR measures the contrast between the tissue of interest and its surroundings to be able to detect the low-contrast details between tissues (consisting mainly of connective tissue, which has a similar density to muscle), so the higher the CNR value, the better. For our purposes, the best image quality, providing the most detailed morphological and structural imaging of hind limb structures was obtained with a bath of 100% ethanol for 14 days.



Scoring of the grayscale values

As CT values correspond to linear X-ray absorption coefficients, voxel grayscale values can be utilized as a linear measure of relative absorption at various points within the sample (Kalender, 2005).

At the end of the 14-day ethanol stain-fixation period, each limb was placed on a gauze and left at room temperature for 20–25 min to allow the ethanol to dry then scanned inside a 50 ml Eppendorf tube where the limb was placed on its anatomical position while the ankle remains in plantar-flexion position. Hind limb ROIs were selected in axial planes using DataViewer software (Bruker v. 1.5), imaging the TA and the tibial tuberosity (Figure 2A). For the calculation of striations, a cross-sectional cut of the animal's leg was made to locate the tibia and fibula. Using Image J (NIH, v 1.53), a region of interest (ROI) was then traced to encompass the tissue between these two bones, utilizing the bones themselves as an anatomical reference. In the sagittal view, the tibial tuberosity was identified to ensure consistent anatomical reference across different specimens when placing the ROI. Within these selected ROIs, grayscale intensities were analyzed and categorized into three regions (Table 1) (Pillen et al., 2009; Engelke et al., 2018; Van den Noort et al., 2022): from 0 to 40 for striations, 41–71 for soft tissue, and 72–255 for bone (Figure 2B). This approach allowed for determining the percentage of the leg area occupied by each type of tissue.

Once the score was established, we proceeded to quantify the fraction corresponding to each tissue type, dividing

it into two regions: (1) the anterior limb compartment inclusive of the TA, extensor digitorum longus (EDL) and extensor hallucis longus (EHL), and (2) the entirety of the hind limb.

Stain-fixation utilizing organic solvents such as alcohol induces protein denaturation through the removal of water from the free carboxyl, hydroxyl, amino, amido and imino groups of the proteins, resulting in tissue shrinkage, protein coagulation, thus a reduction of muscle mass, muscle volume and fiber cross-sectional area (Howat and Wilson, 2014; Leonard et al., 2021). Tissue shrinkage is observed at the same percentage in C and Imm as all samples were subjected to the same alcohol stain-fixation method (data not shown) (Patzelt et al., 2019; Leonard et al., 2021). We used the change in striation area fraction as an indicator of muscle degeneration (Figure 2C) (Martínez-Gutiérrez and García-Pelagio, 2023). Tibia and fibula bone (also called peroneal bone) were also analyzed.

Statistic

All values were reported as mean \pm SD. Statistical significance was assessed with a two-tailed Student's *t* and one-way ANOVA tests and Tukey's *post-hoc* analysis. $*P < 0.05$ was considered statistically significant.

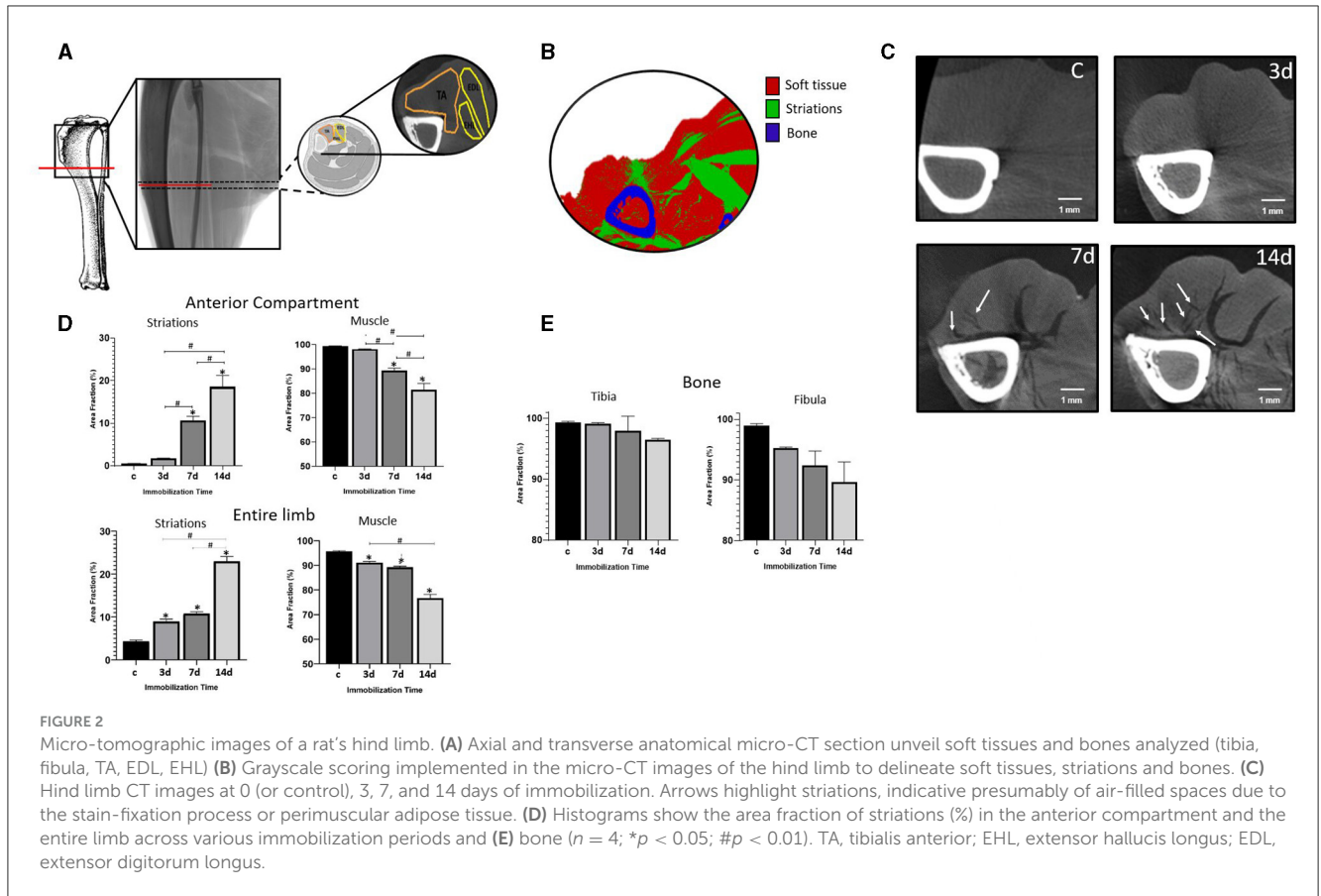


TABLE 1 A grayscale scoring system applied to the hind limb delineates striations, soft tissue and bone.

Tissue	Grayscale value
Striations (air)	0–40
Soft tissue (muscle, fat, connective tissue)	41–71
Bone	72–255

Results

We conducted analysis on both the anterior and posterior muscle compartments (Juneja and Hubbard, 2021; Baan and Maas, 2023) using thermography, while focusing specifically on the anterior limb muscles (TA, EDL and EHL) for micro-CT imaging.

Thermography

Thermograms were obtained in both prone and supine positions at 3, 7, and 14 d of immobilization (Imm) (see Figures 1C, D). The TA was imaged in the supine position, encompassing the cardiac, thoracic, and abdominal organs, areas with the highest blood influx. Conversely, the gastrocnemius was exposed in the prone position, including the back muscles and spine. We observed an increase in temperature throughout the entire hind limb

as the duration of immobilization progressed. While all three sections (proximal, intermediate, and distal) were analyzed in both positions, significant changes were primarily noted in the intermediate prone position, with temperature increases of 4.3, 4.6, and 4.9% ($p < 0.05$) at 3, 7, and 14 days, respectively, compared to the control (see Figures 1C, E). In the supine position (Figures 1D, E), temperature increments were 3.7, 5.3, and 8.6% ($p < 0.05$) for 3, 7, and 14 days, respectively. Also, a significant difference of 1.5% was observed between 3 and 7 d, while a 3.0% difference was noted between 7 and 14 d. In both prone and supine positions, the distal region exhibited lower temperature values compared to the intermediate one, largely due to rodents' tendency to dissipate body heat through their tail, ears, and paws (Dárdai and Heavner, 1989). Furthermore, placing rodents in the supine position, which has a higher temperature threshold, exposed their vital organs to the infrared (IR) chamber. This exposure occurs partly because rodents have a narrow range of thermoregulated core body temperature, which requires significant energy expenditure for maintenance (Reitman, 2018).

Microtomography

We analyzed the anterior compartment and the entire hind limb under *ex vivo* conditions. Qualitative differences in morphology between control and immobilized hind limbs can be observed at 3, 7, and 14 d (see Figure 2C). The main difference

observed was the appearance of dark areas, likely representing air and possible residual perimuscular adipose tissue in smaller quantities, within the soft tissues (muscle, fat, connective tissue). These areas, known as striations, varied depending on the duration of immobilization. Employing grayscale scoring (see Table 1) to quantify the percentage area of striations in the regions of interest (soft tissue, bone, and striations) of the anterior compartment, we observed a higher % area of striations at 14, 7, and 3 d, resulting in increases of up to 18.3, 10.1, and 1.2% ($p < 0.05$), respectively, compared to the control (see Figure 2D). Similarly, for the entire limb, differences of 4.8, 6.8, and 19.9% ($p < 0.05$) were noted at 3, 7, and 14 d, respectively, compared to the control (Figure 2D). Figure 2E illustrates the area fraction of the tibia and fibula bones, revealing a reduction of up to 8.0% at 14 d in the fibula, although not statistically significant. Thus, utilizing alcohol stain-fixative as an alternative to contrast agents enabled quantification of structural changes in the hind limb.

Discussion

Thermography and tomography, are two accessible, rapid and accurate imaging techniques that provide physiological and structural information useful for studying skeletal muscle after induced disuse atrophy caused by periods of immobilization. These techniques can complement other diagnostic methods like magnetic resonance or ultrasound.

Infrared thermography

Our investigation shows that temperature increases over time during the immobilization phase, which is likely due to increased blood flow to the injured area. This increased blood perfusion potentially enhances protein and immune cell release into damaged tissue, leading to vessel dilation, redness, and elevated heat levels—a hallmark of the inflammatory response (Kumar et al., 2007). Such temperature increments play a pivotal role in initiating muscle mass loss, i.e., atrophy (Appell, 1990; Crossland et al., 2019; Ji and Yeo, 2019; Sharlo et al., 2021; Ji et al., 2022). Prolonged immobilization, particularly with a non-functional cast as employed in our study, may exacerbate inflammation associated with tissue damage and temperature elevation (Ohmichi et al., 2012; Całkosiński et al., 2015; Crossland et al., 2019; Parker et al., 2022). This temperature surge is integral to the muscle injury-repair cascade, facilitating either neutrophil invasion through satellite cell activation, triggering factors conducive to muscle repair, or macrophage infiltration followed by muscle lysis, culminating in muscle damage. In both scenarios, inflammatory fibers extravasate into the injured muscle (Best and Hunter, 2000; Tidball, 2005).

In alignment with our findings, Levet et al. (2009) employed static thermography to demonstrate temperature discrepancies between casted and healthy horse limbs, intensifying the temperature over time. Ohmichi et al. (2012) reported an inflammatory response in an immobilized rat hind limb model, inducing muscle atrophy and sustained inflammatory alterations for 1 week. Tomiya et al. observed induction of whole-body thermogenesis in C57Bl/6J mice post-cast removal (Tomiya et al.,

2019). Terkelsen et al. investigated skin temperature changes in the arms of 30 patients following 0, 3, and 28 days of immobilization, revealing significant temperature variations between the control and immobilized hand post-cast removal (Terkelsen et al., 2008). In contrast, Hamaue et al. noted no paw temperature alterations after 1, 2, 3, or 4 weeks of immobilization, potentially attributed to the small size (mm) of the temperature probe placed in the middle of the ipsilateral hind paw (Hamaue et al., 2013).

In summary, thermography emerges as a non-contact, non-invasive, cost-effective modality capable of detecting temperature fluctuations within musculature, signifying abnormal physiological processes, particularly inflammatory responses linked to muscle induced atrophy. Thus, it can be promising as a potential diagnostic tool.

Micro-CT images

We utilized a grayscale scoring system to quantify tissue and bone percentage area (Pillen et al., 2009; Robins et al., 2019), facilitated by ethanol fixation, an economical stain-fixative enabling detailed visualization of hind limb structures, encompassing soft tissue, bone, and striations comparable to other quantitative analyses in tomographic imaging based on anatomical region segmentation utilizing a defined threshold of Hounsfield units (HU) (Bal and Lowe, 2008; Martin et al., 2013; Van der Werf et al., 2017). While ethanol fixation induces dehydration, intrinsic tissue shrinkage (Rolls, 2011; Patzelt et al., 2019; Leonard et al., 2021) and potentially minor alterations in muscle distribution, it affects both control (C) and immobilized (Imm) limbs proportionally, hence not impacting our results. The appearance of striations depended on the duration of immobilization, as muscles tend to diminish in size during muscle atrophy (sarcopenia) (Bonaldo and Sandri, 2013). Longer immobilization periods correlated with increased striations in muscle tissue. Thus, ethanol aids in enhancing tissue visualization, offering an indicator of volume loss in limb muscles (Rolls, 2011; Shirai et al., 2014; Patzelt et al., 2019; Li et al., 2022). Consequently, the ethanol stain-fixation protocol emerges as a viable alternative to contrast agents for *ex-vivo* tissue visualization.

In line with other studies, immobilization precipitates muscle area reduction, accompanied by a decline in muscle strength (Booth, 1987; Clark et al., 2008; Mañas-García et al., 2020; Yopez-Yanez, 2023). This is confirmed by short or prolonged periods of immobilization, hind limb muscle volume undergoes changes, manifesting as reductions in the tibialis anterior (TA), gastrocnemius, soleus, or the entire limb, ranging from 3 to 86% over periods of 3–28 days (Summers and Hines, 1951; Spector et al., 1982; Paun et al., 2020; Yopez-Yanez, 2023). The considerable variability in reported muscle area reduction post-immobilization across studies may stem from differences in imaging acquisition techniques.

These findings are corroborated by other authors utilizing histology (H&E, ATPase, Masson's trichrome, NAD-H), transcriptomics, genomics, or micro-CT analysis with contrast agents (Summers and Hines, 1951; Booth, 1977; Spector et al., 1982; Dupont et al., 2003; Krawiec et al., 2005; Slimani et al., 2015; Pasetto et al., 2018; Paun et al., 2020; Thompson et al., 2022).

Immobilization has been shown to impact bone modeling and remodeling by augmenting the activation of remodeling loci while diminishing osteoblastic stimulus. This heightened activation exacerbates bone formation deficit, directly precipitating local reductions in bone mineral content and density (Minaire, 1989; Kannus et al., 1996; Qian and Hu, 2024). Moreover, a direct correlation exists between bone loss and immobilization, fostering inflammation and bone atrophy (Hardt, 1972; Steinberg, 1980; Minaire, 1989; Tidball, 2005; Brent et al., 2021; Koseki et al., 2022). Following immobilization, immediate bone loss occurs in both trabecular and cortical components, as evidenced by histology and bone ash weights in murine (Tuukkanen et al., 1991; Peng et al., 2021; Rolvien and Amling, 2022) or human tissue (Wiewiorski et al., 2012). This aligns with our observed reduction in the tibia and fibula area fraction, though these results did not reach statistical significance.

Utilizing rapid and cost-effective imaging methods to delineate morphological shifts in skeletal muscle post-injury confers significant advantages in clinical practice. To our knowledge, while thermography has been employed for disease detection, diagnosis, and status assessment, our study marks the progression of muscle inflammation-repair processes following immobilization-induced disuse atrophy. Additionally, quantitative micro-CT imaging, without contrast agents, holds pivotal potential in elucidating animal models of muscle injury, sarcopenia, cachexia, and other muscle-related ailments. IR and micro-CT techniques, similar to ultrasound or MRI, synergistically complement each other, facilitating confident diagnosis and quantification of injury severity.

Integrating infrared imaging and micro-CT into diagnostic practices provides additional insights compared to traditional methods. This approach reveals changes in muscle tissue structure and allows for more efficient assessment across various animal disease models.

Data availability statement

The original contributions presented in the study are included in the article/supplementary material, further inquiries can be directed to the corresponding author.

References

- Aboushady, M. A., Talaat, W., Hamdoon, Z., Elshazly, T., Ragy, N., Bouraue, C., et al. (2021). Thermography as a non-ionizing quantitative tool for diagnosing periapical inflammatory lesions. *BMC Oral Health* 21:260. doi: 10.1186/s12903-021-01618-9
- Al-Nakhli, H. H., Petrofsky, J. S., Laymon, M. S., and Berk, L. S. (2012). The use of thermal infra-red imaging to detect delayed onset muscle soreness. *J. Vis. Exp.* 3551. doi: 10.3791/3551-v
- Appell, H. J. (1990). Muscular atrophy following immobilisation. A review. *Sports Med.* 10, 42–58. doi: 10.2165/00007256-199010010-00005
- Ayala-Domínguez, L., and Brandan, M. E. (2018). Quantification of tumor angiogenesis with contrast-enhanced x-ray imaging in preclinical studies: a review. *Biomed. Phys. Eng. Express.* 4:062001. doi: 10.1088/2057-1976/aadc2d
- Baan, G. C., and Maas, H. (2023). Three-dimensional interactive graphical model of the hindlimb muscles of the rat. *Cells Tissues Organs* 212, 215–219. doi: 10.1159/000523708
- Bal, B. S., and Lowe, J. A. (2008). Muscle damage in minimally invasive total hip arthroplasty: MRI evidence that it is not significant. *Instr. Course Lect.* 57, 223–229.
- Barret, T., Kobayashi, H., Brechbiel, M., and Choyke, P. L. (2006). Macromolecular MRI contrast agents for imaging tumor angiogenesis. *Eur. J. Radiol.* 60, 353–366. doi: 10.1016/j.ejrad.2006.06.025
- Best, T. M., and Hunter, K. D. (2000). Muscle injury and repair. *Phys. Med. Rehabil. Clin. N. Am.* 11, 251–266. doi: 10.1016/S1047-9651(18)30128-1
- Boerckel, J. D., Mason, D. E., McDermott, A. M., and Alsberg, E. (2014). Microcomputed tomography: approaches and applications in bioengineering. *Stem Cell Res. Ther.* 5:144. doi: 10.1186/srct534
- Bonaldo, P., and Sandri, M. (2013). Cellular and molecular mechanisms of muscle atrophy. *Dis. Model. Mech.* 6, 25–39. doi: 10.1242/dmm.010389
- Booth, F. W. (1977). Time course of muscular atrophy during immobilization of hindlimbs in rats. *J. Appl. Physiol. Environ. Exerc. Physiol.* 43, 656–661. doi: 10.1152/jappl.1977.43.4.656

Ethics statement

The animal study was approved by IACUC of the School of Sciences-UNAM according to the Mexican Official Norm (NOM-062-ZOO-1999). The study was conducted in accordance with the local legislation and institutional requirements.

Author contributions

BM-G: Writing – review & editing, Formal analysis, Methodology, Investigation. KG-P: Writing – review & editing, Conceptualization, Funding acquisition, Investigation, Resources, Supervision, Visualization, Writing – original draft.

Funding

The author(s) declare financial support was received for the research, authorship, and/or publication of this article. This work was partially supported by CONAHCYT (S1-17636) and PAPIIT-DGAPA-UNAM (IN 217922) to KG-P.

Conflict of interest

The authors declare that the research was conducted in the absence of any commercial or financial relationships that could be construed as a potential conflict of interest.

Publisher's note

All claims expressed in this article are solely those of the authors and do not necessarily represent those of their affiliated organizations, or those of the publisher, the editors and the reviewers. Any product that may be evaluated in this article, or claim that may be made by its manufacturer, is not guaranteed or endorsed by the publisher.

- Booth, F. W. (1987). Physiologic and biochemical effects of immobilization on muscle. *Clin. Orthop. Relat. Res.* 219, 15–20. doi: 10.1097/00003086-198706000-00004
- Boutin, R., Kaptuch, J., Bateni, C., Chalfant, J., and Yao, L. (2016). Influence of IV contrast administration on CT measures of muscle and bone attenuation: implications for sarcopenia and osteoporosis evaluation. *Am. J. Roentgenol.* 207, 1046–1054. doi: 10.2214/AJR.16.16387
- Brent, M. B., Brüel, A., and Thomsen, J. S. (2021). A systematic review of animal models of disuse-induced bone loss. *Calcif. Tissue Int.* 108, 561–575. doi: 10.1007/s00223-020-00799-9
- Bushberg, J., and Boone, J. (2011). *The Essential Physics of Medical Imaging*. Philadelphia, PA: Lippincott Williams & Wilkins.
- Calkosiński, I., Dobrzyński, M., Rosińczuk, J., Dudek, K., Chrószcz, A., Katarzyna, F., et al. (2015). The use of infrared thermography as a rapid, quantitative, and noninvasive method for evaluation of inflammation response in different anatomical regions of rats. *Biomed Res. Int.* 2015:972535. doi: 10.1155/2015/972535
- Cantillo-Negrete, J., Cuevas-Valencia, R. E., and Alonso, G. A. (2021). Computer-aided diagnosis based on hand thermal, RGB images, and grip force using artificial intelligence as screening tool for rheumatoid arthritis in women. *Med. Biol. Eng. Comput.* 59, 287–300. doi: 10.1007/s11517-020-02294-7
- Clark, B. C., Hoffman, R. L., and Russ, D. W. (2008). Immobilization-induced increase in fatigue resistance is not explained by changes in the muscle metaboreflex. *Muscle Nerve* 38, 1466–1473. doi: 10.1002/mus.21127
- Clark, B. C., Taylor, J. L., Hoffman, R. L., Dearth, D. J., and Thomas, J. S. (2010). Cast immobilization increases long-interval intracortical inhibition. *Muscle Nerve* 42, 363–372. doi: 10.1002/mus.21694
- Cormode, D. P., Naha, P. C., and Fayad, Z. A. (2014). Nanoparticle contrast agents for computed tomography: a focus on micelles. *Contrast Media Mol. Imaging* 9, 37–52. doi: 10.1002/cmmi.1551
- Crossland, H., Skirrow, S., Puthuchery, Z. A., Constantin-Teodosiu, D., and Greenhaff, P. L. (2019). The impact of immobilisation and inflammation on the regulation of muscle mass and insulin resistance: different routes to similar end-points. *J. Physiol.* 597, 1259–1270. doi: 10.1113/JP275444
- Dárdai, E., and Heavner, J. E. (1989). Comparison of respiratory and cardiovascular effects of halothane, isoflurane, and enflurane delivered via the Jackson-Rees breathing system in rats. new anaesthesia model for small animal surgery. *Z. Exp. Chir. Transplant. Neue Organische Organe.* 22, 50–54.
- Descamps, E., Sochacka, A., De Kegel, B., Van Loo, D., Van Hoorebeke, L., and Adriaens, D. (2020). Soft tissue discrimination with contrast agents using micro-CT scanning. *Belg. J. Zool.* 144. doi: 10.26496/bjz.2014.63
- dos Santos Bunn, P., Kopke, M. E., Rodriguez, A. I., De Souza, R., Borba, E., and Bezerra, E. (2020). Infrared thermography and musculoskeletal injuries: a systematic review with meta-analysis. *Infrared Phys. Tech.* 109:103435. doi: 10.1016/j.infrared.2020.103435
- Dudak, J., Zemlicka, J., Karch, J., Patzelt, M., Mrzilkova, J., Zach, P., et al. (2016). High-contrast X-ray micro-radiography and micro-CT of *ex vivo* soft tissue murine organs utilizing ethanol fixation and large area photon-counting detector. *Sci. Rep.* 6:385. doi: 10.1038/srep30385
- Dupont, A., Richmond, J. R., and Loeb, G. E. (2003). Effects of muscle immobilization at different lengths on tetrodotoxin-induced disuse atrophy. *IEEE Transact. Neural Syst. Rehabil. Eng.* 11, 209–217. doi: 10.1109/TNSRE.2003.817675
- Edmund, J. M., and Nyholm, T. (2017). A review of substitute CT generation for MRI-only radiation therapy. *Radiat. Oncol.* 12:28. doi: 10.1186/s13014-016-0747-y
- Engelke, K., Museyko, O., Wang, L., and Laredo, J. D. (2018). Quantitative analysis of skeletal muscle by computed tomography imaging-State of the art. *J. Orthop. Translat.* 28, 91–103. doi: 10.1016/j.jot.2018.10.004
- Faraji, J., Ambeskovic, M., Sauter, N., Toly, J., Whitten, K., Lopes, N. A., et al. (2022). Sex-specific stress and biobehavioral responses to human experimenters in rats. *Front. Neurosci.* 16:965500. doi: 10.3389/fnins.2022.965500
- Findakly, S., Zia, A., Kavnaudias, H., Mathew, J., Varma, D., Di Muzio, B., et al. (2023). The use of whole-body trauma CT should be based on mechanism of injury: a risk analysis of 3920 patients at a tertiary trauma centre. *Injury* 54:59. doi: 10.1016/j.injury.2023.05.059
- Florkow, M. C., Willemsen, K., Mascarenhas, V. V., Oei, E. H. G., van Stralen, M., and Seevinck, P. R. (2022). Magnetic resonance imaging versus computed tomography for three-dimensional bone imaging of musculoskeletal pathologies: a review. *J. Magn. Reson. Imaging* 56, 11–34. doi: 10.1002/jmri.28067
- Hakki, S. S., Götz, W., Dundar, N., Kayis, S. A., Malkoc, S., Hamurcu, M., et al. (2021). Borate and boric acid supplementation of drinking water alters teeth and bone mineral density and composition differently in rabbits fed a high protein and energy diet. *J. Trace Elements Med. Biol.* 67:126799. doi: 10.1016/j.jtemb.2021.126799
- Hallouard, F., Anton, N., Choquet, P., Constantinesco, A., and Vandamme, T. (2010). Iodinated blood pool contrast media for preclinical X-ray imaging applications - a review. *Biomaterials* 31, 6249–6268. doi: 10.1016/j.biomaterials.2010.04.066
- Hamaue, Y., Nakano, J., Sekino, Y., Chuganji, S., Sakamoto, J., Yoshimura, T., et al. (2013). Immobilization-induced hypersensitivity associated with spinal cord sensitization during cast immobilization and after cast removal in rats. *J. Physiol. Sci.* 63, 401–408. doi: 10.1007/s12576-013-0277-4
- Hardt, A. B. (1972). Early metabolic responses of bone to immobilization. *J. Bone Jt. Surg.* 54A:119. doi: 10.2106/00004623-197254010-00011
- Howat, W. J., and Wilson, B. A. (2014). Tissue fixation and the effect of molecular fixatives on downstream staining procedures. *Methods* 70, 12–19. doi: 10.1016/j.jymeth.2014.01.022
- Huang, Z., Fang, Q., and Ma, W. (2019). Skeletal muscle atrophy was alleviated by salidroside through suppressing oxidative stress and inflammation during denervation. *Front. Pharmacol.* 10:997. doi: 10.3389/fphar.2019.00997
- Hussain, O., Kaushal, M., Agarwal, N., Kurpad, S., and Shabani, S. (2023). The role of magnetic resonance imaging and computed tomography in spinal cord injury. *Life* 13:1680. doi: 10.3390/life13081680
- Ilo, A., Romsis, P., and Mäkelä, J. (2020). Infrared thermography as a diagnostic tool for peripheral artery disease. *Adv. Skin Wound Care* 33, 482–488. doi: 10.1097/01.ASW.0000694156.62834.8b
- Ji, L., and Yeo, D. (2019). Cellular mechanism of immobilization-induced muscle atrophy: a mini review. *Sports Med. Health Sci.* 1, 19–23. doi: 10.1016/j.smhs.2019.08.004
- Ji, Y., Li, M., Chang, M., Liu, R., Qiu, J., Wang, K., et al. (2022). Inflammation: roles in skeletal muscle atrophy. *Antioxidants* 11:1686. doi: 10.3390/antiox11091686
- Johnson, J. T., Hansen, M. S., Wu, L., Healy, L. J., Johnson, C. R., Jones, G. M., et al. (2006). Virtual histology of transgenic mouse embryos for high-throughput phenotyping. *PLoS Genet.* 2:e61. doi: 10.1371/journal.pgen.0020061
- Juneja, P., and Hubbard, J. (2021). *Anatomy, Bony Pelvis and Lower Limb: Tibialis Anterior Muscles*. Treasure Island, FL: StatPearls. Available online at: <https://www.ncbi.nlm.nih.gov/books/NBK513304/> (accessed December, 2023).
- Kalender, W. A. (2005). *Computed Tomography: Fundamentals, System Technology, Image Quality, Applications*. Erlangen: Publicis Corporate Publishing.
- Kannus, P., Järvinen, T. L., Sievänen, H., Kvist, M., Rauhaniemi, J., Maunu, V., et al. (1996). Effects of immobilization, three forms of remobilization, and subsequent deconditioning on bone mineral content and density in rat femora. *J. Bone Miner. Res.* 11, 1339–1346. doi: 10.1002/jbmr.5650110919
- Keszytüs, D., Brucher, S., Wilson, C., and Keszytüs, T. (2023). Use of infrared thermography in medical diagnosis, screening, and disease monitoring: a scoping review. *Medicina* 59:2139. doi: 10.3390/medicina59122139
- Koseki, H., Osaki, M., Honda, Y., Sunagawa, S., Imai, C., Shida, T., et al. (2022). Progression of microstructural deterioration in load-bearing immobilization osteopenia. *PLoS ONE* 17:e0275439. doi: 10.1371/journal.pone.0275439
- Krawiec, B. J., Frost, R. A., Vary, T. C., Jefferson, L. S., and Lang, C. H. (2005). Hindlimb casting decreases muscle mass in part by proteasome-dependent proteolysis but independent of protein synthesis. *Am. J. Physiol. Endocrinol. Metab.* 289, E969–E980. doi: 10.1152/ajpendo.00126.2005
- Kumar, V., Abbas, A. K., Fausto, N., and Mitchell, R. N. (2007). *Acute and Chronic Inflammation*. Saunders (Elsevier). *Robbins & Cotran Pathologic Basis of Disease*. New York, NY: McGraw-hill Interamericana.
- Lahiri, B. B., Bagavathiappan, S., Jayakumar, T., and Philip, J. (2012). Medical applications of infrared thermography: a review. *Infrared Phys. Tech.* 55, 221–235. doi: 10.1016/j.infrared.2012.03.007
- Lalwani, K., Giddabasappa, A., Li, D., Olson, P., Simmons, B., Shojaei, F., et al. (2013). Contrast agents for quantitative microCT of lung tumors in mice. *Comp. Med.* 63, 482–490.
- Leonard, K. C., Worden, N., Boettcher, M. L., Dickinson, E., and Hartstone-Rose, A. (2021). Effects of long-term ethanol storage on muscle architecture. *Anat. Rec.* 305, 184–198. doi: 10.1002/ar.24638
- Levet, T., Martens, A., Devisscher, L., Duchateau, L., Bogaert, L., and Vlaminck, L. (2009). Distal limb cast sores in horses: risk factors and early detection using thermography. *Eq. Vet. J.* 41, 18–23. doi: 10.2746/042516408X343046
- Li, M., Lu, S., Huang, P., Xia, T., Yu, Z., Jiang, W., et al. (2022). High-quality, large-scale, semi-thin, & ultra-thin sections of the optic nerve in large animals: an optimized procedure. *Exp. Eye Res.* 219:108956. doi: 10.1016/j.exer.2022.108956
- Lortie, J., Gage, G., Rush, B., Heymsfield, S. B., Szczykutowicz, T. P., and Kuchnia, A. J. (2022). The effect of computed tomography parameters on sarcopenia and myosteatosis assessment: a scoping review. *J. Cach. Sarcop. Muscle* 13, 2807–2819. doi: 10.1002/jcsm.13068
- Lusic, H., and Grinstaff, M. W. (2013). X-ray-computed tomography contrast agents. *Chem. Rev.* 113, 1641–1666. doi: 10.1021/cr200358s
- Mañas-García, L., Penedo-Vázquez, A., López-Postigo, A., Deschrevel, J., Durán, X., and Barreiro, E. (2020). Prolonged immobilization exacerbates the loss of muscle mass and function induced by cancer-associated cachexia through enhanced proteolysis in mice. *Int. J. Mol. Sci.* 21:8167. doi: 10.3390/ijms2118167
- Martin, L., Birdsell, L., MacDonald, N., Reiman, T., Clandinin, M. T., McCargar, L. J., et al. (2013). Cancer cachexia in the age of obesity: skeletal muscle depletion

- is a powerful prognostic factor independent of body mass index. *J. Clin. Oncol.* 31, 1539–1547. doi: 10.1200/JCO.2012.45.2722
- Martínez-Gutiérrez, B. A., and García-Pelagio, K. P. (2023). Study of hind limb skeletal muscles in rats after immobilization using microCT and thermographic imaging. *AIP Conf. Proc.* 2947:030018. doi: 10.1063/5.0161249
- Metscher, B. D. (2009). MicroCT for developmental biology: a versatile tool for high-contrast 3D imaging at histological resolutions. *Dev. Dyn.* 238, 632–640. doi: 10.1002/dvdy.21857
- Minaire, P. (1989). Immobilization osteoporosis: a review. *Clin. Rheumatol.* 2(Suppl.), 95–103. doi: 10.1007/BF02207242
- Nishide, K., Nagase, T., Oba, M., Oe, M., Ohashi, Y., Iizaka, S., et al. (2009). Ultrasonographic and thermographic screening for latent inflammation in diabetic foot callus. *Diabetes Res. Clin. Pract.* 85, 304–309. doi: 10.1016/j.diabres.2009.05.018
- Ohmichi, Y., Sato, J., Ohmichi, M., Sakurai, H., Yoshimoto, T., Morimoto, A., et al. (2012). Two-week cast immobilization induced chronic widespread hyperalgesia in rats. *Eur. J. Pain.* 16, 338–348. doi: 10.1002/j.1532-2149.2011.00026.x
- O'Sullivan, J. D. B., Behnsen, J., Starborg, T., MacDonald, A. S., Phythian-Adams, A. T., Else, K. J., et al. (2018). X-ray micro-computed tomography (μ CT): an emerging opportunity in parasite imaging. *Parasitology* 145, 848–854. doi: 10.1017/S0031182017002074
- Parker, E., Khayrullin, A., Kent, A., Mendhe, B., Youssef El Baradie, K. B., Yu, K., et al. (2022). Hindlimb immobilization increases IL-1 β and Cdkn2a expression in skeletal muscle fibro-adipogenic progenitor cells: a link between senescence and muscle disuse atrophy. *Front. Cell Dev. Biol.* 9:790437. doi: 10.3389/fcell.2021.790437
- Pasetto, L., Olivari, D., Nardo, G., Trolese, M. C., Bendotti, C., Piccirillo, R., et al. (2018). Micro-computed tomography for non-invasive evaluation of muscle atrophy in mouse models of disease. *PLoS ONE* 13:e0198089. doi: 10.1371/journal.pone.0198089
- Pasternak, J. J., and Williamson, E. E. (2012). Clinical pharmacology, uses, and adverse reactions of iodinated contrast agents: a primer for the non-radiologist. *Mayo Clin. Proc.* 87, 390–402. doi: 10.1016/j.mayocp.2012.01.012
- Patzelt, M., Mrzilkova, J., Dudak, J., Krejci, F., Zemlicka, J., Karch, J., et al. (2019). Ethanol fixation method for heart and lung imaging in micro-CT. *Jpn. J. Radiol.* 37, 500–510. doi: 10.1007/s11604-019-00830-6
- Paun, B., Leon, D. G., Cabello, A. C., Pages, R. M., de la Calle Vargas, E., Muñoz, P. C., et al. (2020). Modelling the skeletal muscle injury recovery using *in vivo* contrast-enhanced micro-CT: a proof-of-concept study in a rat model. *Eur. Radiol. Exp.* 4:33. doi: 10.1186/s41747-020-00163-4
- Pauwels, R., Silkosessak, O., Jacobs, R., Bogaerts, R., Bosmans, H., and Panmekiate, S. (2014). A pragmatic approach to determine the optimal kVp in cone beam CT: balancing contrast-to-noise ratio and radiation dose. *Dentomaxillofac. Radiol.* 43:20140059. doi: 10.1259/dmfr.20140059
- Peng, X., Qu, Y., and Li, X. (2021). Bone mineral density and its influencing factors in Chinese children with spinal muscular atrophy types 2 and 3. *BMC Musculoskelet. Disord.* 22:729. doi: 10.1186/s12891-021-04613-x
- Pillen, S., van Dijk, J. P., Weijers, G., Rajimman, W., de Korte, C. L., and Zwarts, M. J. (2009). Quantitative gray-scale analysis in skeletal muscle ultrasound: a comparison study of two ultrasound devices. *Muscle Nerve* 39, 781–786. doi: 10.1002/mus.21285
- Polyaev, A. Y., Tyagunov, A. E., Polonsky, A. A., Vinogradov, V. N., Trudkov, D. Y., Mosin, S. V., et al. (2018). Of mice and men - environmental temperature, body temperature, and treatment of obesity. *FEBS Lett.* 592, 2098–2107. doi: 10.1002/1873-3468.13070
- Qian, A., and Hu, L. (2024). *Bone Cell Biomechanics, Mechanobiology and Bone Diseases*. Academic Press, 31–52. doi: 10.1016/C2021-0-01878-2
- Reitman, M. L. (2018). Of mice and men - environmental temperature, body temperature, and treatment of obesity. *FEBS Lett.* 592, 2098–2107.
- Robins, M., Solomon, J., Hurwitz, L., Christensen, J., and Samei, E. (2019). Validation of lesion simulations in clinical CT data for anonymized chest and abdominal CT databases. *Med. Phys.* 46, 1931–1937. doi: 10.1002/mp.13412
- Robinson, P. M., and O'Meara, M. J. (2009). The Thomas splint: its origins and use in trauma. *J. Bone Joint Surg. Br.* 1, 540–544. doi: 10.1302/0301-620X.91B4.21962
- Rolls, G. (2011). *Fixation and Fixatives (2) – Factors Influencing Chemical Fixation, Formaldehyde and Glutaraldehyde*. Deer Park, IL: Leica Biosystems Publications.
- Rolvien, T., and Amling, M. (2022). Disuse osteoporosis: clinical and mechanistic insights. *Calc. Tissue Intl.* 110, 592–604. doi: 10.1007/s00223-021-00836-1
- Sachse, A., Leike, J. U., Schneider, T., Wagner, S. E., Rossling, G. L., Krause, W., et al. (1997). Biodistribution and computed tomography blood-pool imaging properties of polyethylene glycol-coated iopromide-carrying liposomes. *Investig. Radiol.* 32, 44–50. doi: 10.1097/00004424-199701000-00007
- Schaad, L., Hlushchuk, R., Barré, S., Gianni-Barrera, R., Haberthur, D., Banfi, A., et al. (2017). Correlative imaging of the murine hind limb vasculature and muscle tissue by MicroCT and light microscopy. *Sci. Rep.* 7:41842. doi: 10.1038/srep41842
- Sharlo, K., Tyganov, S. A., Tomilovskaya, E., Popov, D. V., Saveko, A. A., and Shenkman, B. S. (2021). Effects of various muscle disuse states and countermeasures on muscle. *Int. J. Mol. Sci.* 23:468. doi: 10.3390/ijms23010468
- Shirai, R., Kunii, T., Yoneyama, A., Ooizumi, T., Maruyama, H., Lwin, T.-T., et al. (2014). Enhanced renal image contrast by ethanol fixation in phase-contrast X-ray computed tomography. *J. Synchr. Radiat.* 21, 795–800. doi: 10.1107/S1600577514010558
- Slimani, L., Vazeille, E., Deval, C., Meunier, B., Polge, C., Dardevet, D., et al. (2015). The delayed recovery of the remobilized rat tibialis anterior muscle reflects a defect in proliferative and terminal differentiation that impairs early regenerative processes. *J. Cach. Sarcop. Muscle* 6, 73–83. doi: 10.1002/jcsm.12011
- Spector, S. A., Simard, C. P., Fournier, M., Strenlicht, V. R., and Edgerton, V. R. (1982). Architectural alterations of rat hind-limb skeletal muscles immobilized at different lengths. *Exp. Neurol.* 76, 94–110. doi: 10.1016/0014-4886(82)90104-2
- Steinberg, F. (1980). *The Immobilized Patient. Functional Pathology and Management*. Springer Nature, 33–63.
- Strandberg, S., Wretling, M. L., Wredmark, T., and Shalabi, A. (2010). Reliability of computed tomography measurements in assessment of thigh muscle cross-sectional area and attenuation. *BMC Med. Imaging* 10:18. doi: 10.1186/1471-2342-10-18
- Summers, T. B., and Hines, H. M. (1951). Effect of immobilization in various positions upon the weight and strength of skeletal muscle. *Arch. Phys. Med.* 32, 142–145.
- Tan, Y. K., Hong, C., Li, H., Allen, J. C., and Thumboo, J. (2020). Thermography in rheumatoid arthritis: a comparison with ultrasonography and clinical joint assessment. *Clin. Radiol.* 75, e17–e963. doi: 10.1016/j.crad.2020.08.017
- Terkelsen, A. J., Bach, F. W., and Jensen, T. S. (2008). Experimental forearm immobilization in humans induces cold and mechanical hyperalgesia. *Anesthesiology* 109, 297–307. doi: 10.1097/ALN.0b013e31817f4c9d
- Thirunavukkarasu, U., Umopathy, S., Janardhanan, K., and Thirunavukkarasu, R. (2020). A computer aided diagnostic method for the evaluation of type II diabetes mellitus in facial thermograms. *Phys. Eng. Sci. Med.* 43, 871–888. doi: 10.1007/s13246-020-00886-z
- Thompson, J. M., West, D. W. D., Doering, T. M., Budiono, B. P., Lessard, S. J., Koch, L. G., et al. (2022). Effect of short-term hindlimb immobilization on skeletal muscle atrophy and the transcriptome in a low compared with high responder to endurance training model. *PLoS ONE* 17:e0261723. doi: 10.1371/journal.pone.0261723
- Tidball, J. G. (2005). Inflammatory processes in muscle injury and repair. *Am. J. Physiol. Regul. Integr. Comp. Physiol.* 288, R345–R353. doi: 10.1152/ajpregu.00454.2004
- Tolonen, A., Pakarinen, T., Sassi, A., Kytä, J., Cancino, W., Rinta-Kiikka, I., et al. (2021). Methodology, clinical applications, and future directions of body composition analysis using computed tomography (CT) images: a review. *Eur. J. Radiol.* 145:109943. doi: 10.1016/j.ejrad.2021.109943
- Tomiya, S., Tamura, Y., Kouzaki, K., Kotani, T., Wakabayashi, Y., Noda, M., et al. (2019). Cast immobilization of hindlimb upregulates sarcolipin expression in atrophied skeletal muscles and increases thermogenesis in C57BL/6j mice. *Am. J. Physiol. Regul. Integr. Comp. Physiol.* 5, R649–R661. doi: 10.1152/ajpregu.00118.2019
- Tuukkanen, J., Wallmark, B., Jalovaara, P., Takala, T., Sjögren, S., and Väänänen, K. (1991). Changes induced in growing rat bone by immobilization and remobilization. *Bone* 12, 113–118. doi: 10.1016/8756-3282(91)90009-8
- Van den Noort, J. C., van der Leeden, M., Stapper, G., Wirth, W., Maas, M., Roorda, L. D., et al. (2022). Muscle weakness is associated with non-contractile muscle tissue of the vastus medialis muscle in knee osteoarthritis. *BMC Musculoskelet. Disord.* 23:91. doi: 10.1186/s12891-022-05025-1
- Van der Werf, A., Langius, J. A. E., de van der Schueren, M. A. E., Nurmohamed, S. A., van der Pant, K. A. M. I., Blauwhoff-Buskermolen, S., et al. (2017). Percentiles for skeletal muscle index, area and radiation attenuation based on computed tomography imaging in a healthy Caucasian population. *Eur. J. Clin. Nutr.* 72, 288–296. doi: 10.1038/s41430-017-0034-5
- Vickerton, P., Jarvis, J., and Jeffery, N. (2013). Concentration-dependent specimen shrinkage in iodine-enhanced microCT. *J. Anat.* 223, 185–193. doi: 10.1111/joa.12068
- Wiewiorski, M., Dopke, K., Steiger, C., and Valderrabano, V. (2012). Muscular atrophy of the lower leg in unilateral post traumatic osteoarthritis of the ankle joint. *Int. Orthopaed.* 36, 2079–2085. doi: 10.1007/s00264-012-1594-6
- Yan, Y., Li, X., Cai, X., and Niu, H. (2012). “Exploration of imaging method of degenerate articular cartilage based on EPIC Micro-CT” in *2012 Int Conf Biomedical Engineering and Biotechnology Macau, Macao* 2012, 797–800.
- Yepez-Yanez, S. G. (2023). *Cambios morfológicos, histológicos y mio-mecánicos en el músculo esquelético de ratones en modelos de inmovilización y entrenamiento muscular* (Master Thesis). Universidad Nacional Autónoma de México, Mexico City, Mexico. Available online at: <http://132.248.9.195/ptd2023/octubre/0849045/Index.html> (accessed March 16, 2024).
- Zaproudina, N., Ming, Z., and Hänninen, O. O. (2006). Plantar infrared thermography measurements and low back pain intensity. *J. Manip. Physiol. Ther.* 29, 219–223. doi: 10.1016/j.jmpt.2006.01.003